Simulation Study on the Dynamics of Cavitation Bubbles in Multi-Frequency Ultrasound

Hu Dong (PhD)[1]*, Gang Liu (PhD)[2], Gaofeng Peng (MD)[1]

[1]School of Information Science and Engineering, Changsha Normal University, Changsha 410100, China
[2]School of Information Science and Engineering, Xinyu University, Xinyu, 338004, China

ABSTRACT

Background: High-intensity focused ultrasound (HIFU) therapy is an effective minimally invasive treatment technique.

Objective: This work aimed to present a theoretical foundation for transient cavitation control in HIFU treatment and investigate cavitation bubbles in multi-frequency ultrasound.

Material and Methods: In this theoretical study, the nonlinear vibrations of bubbles in different mediums (water, urine, kidney, and muscle) were simulated using Gilmore-Akulichev and modified Keller-Miksis equations. The dynamic changes of bubble radius during irradiation by multi-frequency combined ultrasound were analyzed, and the effects of multi-frequency ultrasound combinations and frequency differences on the maximum and minimum values of bubble expansion radius and bubble collapse time were investigated.

Results: At the same highest frequency, the triple-frequency produced the largest bubble expansion radius (R_{max}) while the single-frequency resulted in the smallest bubble expansion radius (R_{min}). At the same lowest frequency, the single-frequency had the biggest bubble expansion radius and the triple-frequency had the smallest bubble expansion radius. Compared to the combination with a large frequency difference at high frequency, the triple-frequency combination with a small frequency difference at low frequency exhibited a noticeably larger R_{max}, but R_{min} showed the opposite behavior. R_{max}/R_{min} decreased for the same ultrasonic combination when the medium viscosity increased. The bubble expansion radius ratio R_{max}/R_{min} was positively correlated with the bubble collapse time.

Conclusion: There was a strong correlation between the frequency difference and the multi-frequency ultrasound combination and the maximum and minimum values of the cavitation bubble radius and the collapse time.

Keywords

High-Intensity Focused Ultrasound; Nonlinear; Transient; Cavitation; Dynamic; Collapse; Viscosity; Ultrasonics; Radius

Introduction

The growth, oscillation, and collapse of bubbles in the medium under ultrasonic irradiation is known as the cavitation effect. This phenomenon can either expand gradually and eventually collapse, or oscillate steadily, which is known as steady-state cavitation [1]. Transient cavitation, which is commonly referred to as cavitation, is influenced by a number of variables, such as the ultrasonic frequency, bubble

*Corresponding author:
Hu Dong
School of Information Science and Engineering, Changsha Normal University, Changsha 410100, China
E-mail: weijundong203@outlook.com

Received: 12 October 2024
Accepted: 22 February 2025

size, and the properties of the surrounding medium [2]. Ultrasonic cavitation generates high temperatures and pressures, which are widely used in the medical field for tumor and thrombosis treatment [3-5]. Compared with conventional single-frequency ultrasound, multi-frequency ultrasound demonstrates two unique advantages in enhancing the cavitation effect, such as lowering the cavitation threshold and increasing response efficiency [6,7].

Ultrasound has been the subject of much research in recent years as a way to introduce energy into a medium and cause chemical and physical changes through the process of bubble collapse [8-10]. A dual-frequency acoustic processor, which has increased cavitation yield, was quantitatively examined by Mohalkar et al. [11], who proposed that the processor's more uniform acoustic field was the cause of the rise in cavitation yield. They also offered a way to achieve homogeneous cavitation intensity in the reactor by optimizing the dual-frequency acoustic field settings. According to Tatake et al.'s numerical analysis [12], the greatest cavitation enhancement is anticipated when a second acoustic wave with the same frequency as the first one is introduced. In their numerical modeling, Servent et al. [13] took into account the spatiotemporal dynamics of cavitation bubbles and nucleation spots in the three-dimensional geometry of an acoustic chemical reactor. They also concluded that multi-frequency systems have a greater cavitation bubble volume fraction (indicating that more cavitation events may occur with a dual-frequency source than with a single-frequency source).

Dual- or multi-frequency ultrasonography has been widely used in recent years to boost sonochemical yield and cavitation intensity [14]. Multi-frequency systems encourage cavitation nucleation more than single-frequency ultrasonic cavitation. Furthermore, bubbles have a higher growth rate with a collapse pressure. Brotchie et al. [15] showed that simultaneous ultrasonic excitation at 20 kHz and 355 kHz greatly increased both acoustoluminescence and sonochemistry. According to Saletes et al. [16], lowering the cavitation threshold for multi-frequency ultrasonic excitation makes it easier for transient cavitation to start. Koufaki et al. [17] significantly shortened the reaction time for the synthesis of 3,5 dimethylisoxazole by dual-frequency ultrasound at 20 kHz and 40 kHz. The transient cavitation threshold of microbubbles under multi-frequency ultrasonic irradiation was examined by Suo et al. [18], who also examined the correlation between the cavitation threshold and microbubble size at various frequencies and media. They put forth a theoretical framework for lowering the cavitation threshold using dual-frequency ultrasonography.

The process is still unclear, despite numerous researchers' experimental confirmation that dual-frequency and multi-frequency ultrasound can enhance cavitation intensity and sonochemical yield [6,7,11,12,14]. Information on cavitation can be efficiently obtained through numerical analysis of cavitation kinetics [19]. More variables, including the frequency and amplitude of each ultrasonic beam, their phase difference, and the power distribution, are present in multi-frequency ultrasonic systems. Cavitation phenomena and bubble oscillations become more intricate as a result.

Khanna et al. [20] explained the spatial distribution of cavitation intensity and the dynamic phase diagram of cavitation using the dual-frequency ultrasound model. They also observed that for the same ultrasonic pressure amplitude, the cavitation strength increased as the dual-frequency ultrasound frequency ratio droped. The impact of dual-frequency ultrasound's frequency and pressure amplitude on heat transfer at the bubble-liquid interface was examined numerically by Zhang et al. [21]. They proposed that cavitation may be more successfully promoted by boosting the power of dual-frequency ultrasound's low-frequency component. The wider frequency spectrum

created by nonlinear mixing of dual-frequency ultrasound was the reason why Guédra et al. [22] used the asymptotic method to analyze the nonlinear vibration of bubbles generated by dual-frequency ultrasound excitation. They discovered that at high enough ultrasound pressures and a specific frequency difference, the response amplitude of the bubbles was larger than that of single-frequency ultrasound excitation. In order to investigate the dynamic evolution of bubbles in single- and dual-frequency ultrasound modes, Ye et al. [23] created a dual-frequency ultrasound cavitation dynamics model. The findings demonstrated that cavitation bubbles oscillate more unstably and collapse more readily in a dual-frequency ultrasound field than in a single-frequency ultrasound field. The cavitation impact is lessened as the ultrasonic frequency rises because of the shorter oscillation period. Azam et al. [24] used multi-frequency (20 kHz, 40 kHz, and 60 kHz) combined ultrasonic modes to remove residual pesticides, such as methomyl from the surface of fresh lettuce and found that the triple-frequency combined modes were more effective in removing the residual pesticides. Liao et al. [25] showed an acoustic cavitation under ultrasonic irradiation is affected by dual-frequency coupling factors, including frequency difference, phase difference, and power distribution ratio. The acoustic cavitation was shown to be significantly impacted by every coupling parameter. While the combination of high and low frequencies easily created an attenuation effect, the mixing of low and low frequencies was discovered to have an augmentation impact for various frequency combinations. In order to promote mass transfer or diffusion, Wang et al. [26] numerically examined the mass transfer behavior of microbubbles in liquids under multi-frequency acoustic excitation with different frequencies, pressure amplitudes, and amplitude ratios. They proposed that the low-frequency component of the multi-frequency acoustic excitation should receive the power because low-frequency acoustic excitation has a more significant effect than high frequency in the growth region.

It is clear from the above studies that multi-frequency ultrasound has an important effect on bubble dynamics, cavitation intensity, and acoustic chemical yield in the ultrasound field. However, the research in this area still needs to be further strengthened. In this paper, a multi-frequency ultrasound bubble dynamics model was developed for four mediums: water, urine, kidney, and muscle. The bubble dynamics equations were used to simulate and analyze the effects of multi-frequency ultrasound combination and frequency difference on the maximum and minimum values of bubble radius and bubble collapse time.

Material and Methods

For this theoretical analysis of fluid (i.e., Water and Urine), the Gilmore-Akulichev formulation of the bubble dynamics is shown in equation (1) below [27]. The computation makes the assumptions that the bubbles stay spherical during the simulation and that nonlinear propagation aberrations do not taint the ultrasonic waves.

$$R(1-\frac{U}{C})\frac{dU}{dt}+\frac{3}{2}(1-\frac{U}{3C})U^2=(1-\frac{U}{C})H+\frac{U}{C}(1-\frac{U}{C})R\frac{dH}{dR} \quad 1$$

The reaction of a single bubble in relation to time is shown by equation (1). The initial radius is represented by R, the first-order derivative with respect to time by U, the speed of sound of the liquid containing the bubble by C, and the enthalpy of that liquid by H. The calculation of equation (1) and its related parameters (such as density ρ, the multivariate exponent κ, the shear coefficient viscosity μ, the surface tension σ) are related to five subequations [28-30].

In contrast, in tissues, such as kidney and muscle, a modified Keller-Miksis equation that takes into account the surrounding tissue's compressibility and viscoelasticity is used to explain the bubble dynamics [31].

$$(1-\frac{\dot{R}}{c})R\ddot{R}+\frac{3}{2}(1-\frac{\dot{R}}{3c})\dot{R}^2=(1+\frac{\dot{R}}{c})[\frac{P_B-P_\infty(t)}{\rho}-\frac{4\mu\dot{R}}{R}-\frac{2\sigma}{\rho R}-E_{NT}]+\frac{R}{\rho c}\frac{d}{dt}(P_a-P_\infty) \quad 2$$

Where c is the constant speed of sound in the tissue, "." denotes the time derivative, and $\ddot{R}$ is the bubble wall acceleration. The tissue's viscoelasticity is modeled using the Kelvin-Voigt method. The hyperelastic constitutive relation is used to obtain the elastic term while taking into account massive deformations during bubble growth [32].

$$E_{NT} = \frac{G}{2}[5 - 4(\frac{R_0}{R}) - (\frac{R_0}{R})^4] \quad 3$$

Where G is the linear shear modulus. For multi-frequency ultrasonic irradiation, the ultrasonic excitation signal can be expressed as:

$$P_s = p_1 \sin(2\pi f_1 t) + \varphi p_2 \sin(2\pi f_2 t + \alpha) + \phi p_3 \sin(2\pi f_3 t + \beta) \quad 4$$

Where f_1, f_2 and f_3 are the excitation signal frequencies, p_1, p_2 and p_3 are the sound pressure amplitudes, $0 \le \phi \le 1$, $0 \le \varphi \le 1$. α and β are the excitation signal phase angles, $0 \le \alpha \le 2\pi$ and $0 \le \beta \le 2\pi$. The ordinary differential equation solver ode45 was used in MATLAB R2018b (MathWorks, Naticks, MA, USA) to determine the transient bubble radius R. The Gilmore-Akulichev and modified Keller-Miksis equations were numerically solved in MATLAB (MathWorks, Naticks, MA, USA) using the fifth-order Runge-Kutta-Fehlberg method and the step control algorithm [27,33,34] with absolute and relative tolerances of 2e-12 and 1e-8, respectively, yielding radius-time parameters of satisfactory accuracy. R_{max}=$2R_0$ can be used as a condition for the occurrence of transient cavitation in order to solve the transient cavitation threshold in the medium [35]. For transient cavitation, the bubble collapse time is defined as the period of time between the bubble's maximum size and its reduction to less than 1% of its initial size [12].

(a)When $\varphi = \phi = 0$, i.e., a single-frequency (f_1) excitation, p_1=p_0,

$$p_s = p_0 \sin(2\pi f_1 t) \quad 5$$

(b)When $\varphi = 1$, φ=0, α=0, i.e., a dual-frequency ($f_1 \neq f_2$) excitation, $p_1 = p_2 = \frac{1}{\sqrt{2}} p_0$,

$$p_s = \frac{1}{\sqrt{2}} p_0 \sin(2\pi f_1 t) + \frac{1}{\sqrt{2}} \sin(2\pi f_2 t) \quad 6$$

(c)When $\varphi = \phi = 1$, α=β=0, i.e., a triple-frequency ($f_1 \neq f_2 \neq f_3$) excitation, $p_1 = p_2 = p_3 = \frac{1}{\sqrt{3}} p_0$,

$$p_s = \frac{1}{\sqrt{3}} p_0 \sin(2\pi f_1 t) + \frac{1}{\sqrt{3}} \sin(2\pi f_2 t) + \frac{1}{\sqrt{3}} \sin(2\pi f_3 t) \quad 7$$

To guarantee that the acoustic power for dual- and triple-frequency excitation is equal to that for single-frequency excitation, the aforementioned factors $\sqrt{2}$ and $\sqrt{3}$ are utilized. Assuming zero velocity at the interface between the first bubble and the surrounding medium ($\dot{R}$=0), the bubble's initial radius ranges from R_0=0.1 μm to 30 μm. Single-frequency, dual-frequency, and triple-frequency ultrasonography are the irradiation modes in the following, unless otherwise noted, and κ is assumed to be 1.4.The physical parameters of urine, water, kidney, and muscle are used for the simulation study of the bubble radius variation and collapse time for all the four mediums as shown in Table 1.

Results

The bubble radii generated by cavitation in the fluid and tissue are shown in Figures 1 and 2 by triple-frequency (1.2+1.8+2.4 MHz, 1.2+1.3+1.4 MHz, 1.2+1.21+1.22 MHz, 0.5+1.1+1.7 MHz, 0.5+0.6+0.7 MHz, and 0.5+0.51+0.52 MHz), dual-frequency (1.2+1.8 MHz and 1.8+2.4 MHz), and single-frequency (1.2 MHz and 2.4 MHz) irradiation of four different medium, the bubble radius generated by cavitation versus time is shown in Figures 1 and 2, and the variation of the bubble radius with time in the fluid and tissues exhibits nonlinear oscillations.

The simulation results show that the bubble radius oscillations are related not only to the surrounding medium, but also to the irradiation frequency. The simulation results of bubble expansion radius maximum (R_{max}), bubble expansion radius minimum (R_{min}), R_{max}/R_{min}, and bubble collapse time (t_c) for different me-

Table 1: Physical parameters of the medium

Medium	Speed/c (m/s)	Density/ρ (kg/m^3)	Surface tension/σ (mN/m)	viscosity/μ (mPa.s	Shear modulus/G (MPa)
Urine [18,36]	1520	1022	60	0.84	0
Water [27,36]	1500	1000	68	1	0
Kidney [27,36]	1561	1100	56	5	0.18
Muscle [18,36]	1549	1100	56	7	0.45

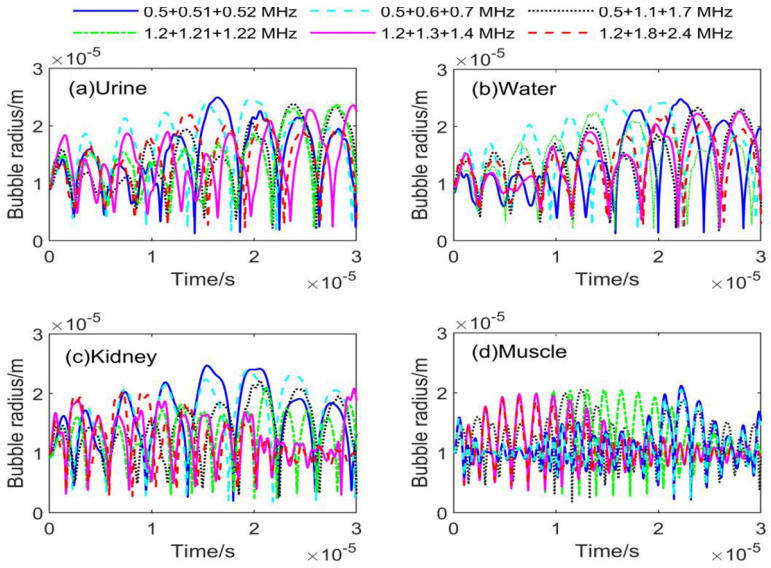

Figure 1: Radius of oscillation of bubbles at different combinations of triple frequency (**a**) Urine; (b) Water; (**c**) Kidney; (**d**) Muscle

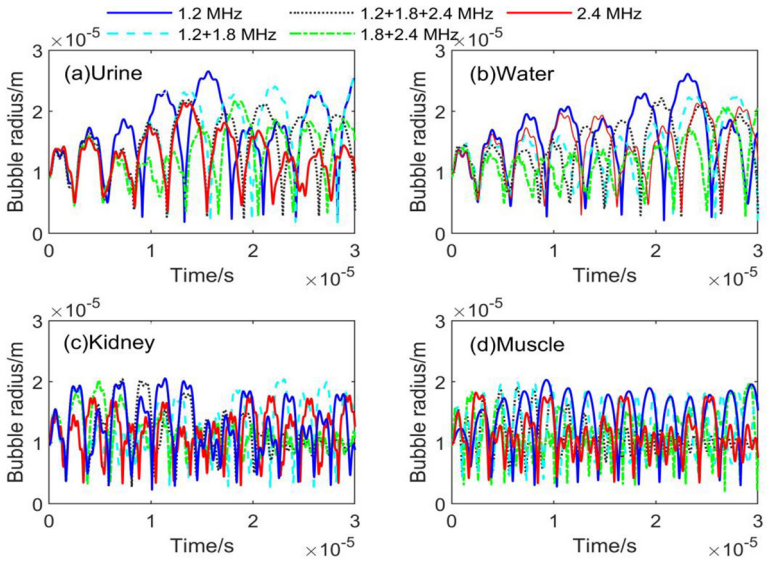

Figure 2: Radius of oscillation of bubbles for single, dual, and triple frequency combinations (**a**) Urine; (**b**) Water; (**c**) Kidney; (**d**) Muscle

dium under different triple-frequency combinations of ultrasonic irradiation are shown in Tables 2 and 3.

The simulation results of bubble expansion radius maximum (R_{max}), bubble expansion radius minimum (R_{min}), R_{max}/R_{min}, and bubble collapse time (t_c) for different medium under different single-frequency, dual-frequency and triple-frequency combinations of ultrasonic irradiation are shown in Tables 4 and 5.

In the same medium, the triple-frequency combinations corresponding to the maximum value of bubble radius from small to large are 1.2+1.8+2.4 MHz, 1.2+1.3+1.4 MHz, 1.2+1.21+1.22 MHz, 0.5+1.1+1.7 MHz, 0.5+0.6+0.7 MHz, and 0.5+0.51+0.52 MHz, while the triple-frequency combinations corresponding to the minimum value of bubble radius from small to large are just the opposite. For the single-frequency, dual-frequency and triple-frequency combinations, the irradiation frequencies corresponding to the maximum values of the bubble radius in descending order are 2.4 MHz, 1.8+2.4 MHz, 1.2+1.8+2.4 MHz, 1.2+1.8 MHz and 1.2 MHz, whereas the minimum values of the bubble radius corresponding to the smallest values of the bubble radius in descending order are just the opposite of the irradiation frequencies. The viscosity of the medium limits the bubble oscillations to some extent, lowering the nonlinearity and amplitude [32].

Table 2: Comparison of bubble radius and collapse time in urine and water at different triple-frequency combinations

Frequency (MHz)	Medium: Urine				Medium: Water			
	R_{max}(μm)	R_{min}(μm)	R_{max}/R_{min}	t_c(μs)	R_{max}(μm)	R_{min}(μm)	R_{max}/R_{min}	t_c(μs)
1.2+1.8+2.4	22.91	2.603	8.80	1.718	22.63	2.915	7.76	1.667
1.2+1.3+1.4	23.58	2.518	9.36	1.881	22.68	2.576	8.80	1.714
1.2+1.21+1.22	23.77	2.474	9.61	1.968	22.79	2.539	8.98	1.823
0.5+1.1+1.7	23.82	2.294	10.38	2.105	23.27	2.324	10.01	1.997
0.5+0.6+0.7	24.60	2.211	11.13	2.273	24.70	2.264	10.91	2.209
0.5+0.51+0.52	24.92	1.394	17.88	4.018	24.78	1.422	17.43	3.980

Table 3: Comparison of bubble radius and collapse time in kidney and muscle at different triple-frequency combinations

Frequency (MHz)	Medium: Kidney				Medium: Muscle			
	R_{max}(μm)	R_{min}(μm)	R_{max}/R_{min}	t_c(μs)	R_{max}(μm)	R_{min}(μm)	R_{max}/R_{min}	t_c(μs)
1.2+1.8+2.4	20.25	3.626	5.58	1.487	19.26	4.052	4.75	1.375
1.2+1.3+1.4	20.99	3.161	6.64	1.549	19.79	3.816	5.19	1.415
1.2+1.21+1.22	21.10	2.925	7.21	2.095	20.13	3.236	6.22	1.506
0.5+1.1+1.7	22.15	2.534	8.70	1.712	20.48	3.113	6.59	1.511
0.5+0.6+0.7	23.41	2.197	10.65	2.183	21.05	3.001	7.01	1.647
0.5+0.51+0.52	24.70	1.990	12.41	2.517	21.17	2.250	9.41	1.942

Table 4: Comparison of bubble radius and collapse time in urine and water for single, dual, and triple-frequency combinations

Frequency (MHz)	Medium: Urine				Medium: Water			
	R_{max}(μm)	R_{min}(μm)	R_{max}/R_{min}	t_c(μs)	R_{max}(μm)	R_{min}(μm)	R_{max}/R_{min}	t_c(μs)
2.4	21.19	3.575	5.93	1.490	20.30	3.683	5.51	1.482
1.8+2.4	21.58	2.875	7.51	1.525	20.61	3.182	6.48	1.518
1.2+1.8+2.4	22.91	2.603	8.80	1.718	22.63	2.915	7.76	1.667
1.2+1.8	25.49	2.190	11.64	2.314	22.76	2.590	8.79	1.714
1.2	26.54	1.874	14.16	2.772	26.13	2.174	12.02	2.421

Table 5: Comparison of bubble radius and collapse time in kidney and muscle for single, dual and triple-frequency combinations

Frequency (MHz)	Medium: Kidney				Medium: Muscle			
	R_{max}(μm)	R_{min}(μm)	R_{max}/R_{min}	t_c(μs)	R_{max}(μm)	R_{min}(μm)	R_{max}/R_{min}	t_c(μs)
2.4	17.99	3.712	4.85	1.382	17.32	4.652	3.72	0.891
1.8+2.4	20.04	3.687	5.44	1.439	18.13	3.923	4.62	1.316
1.2+1.8+2.4	20.25	3.626	5.58	1.487	19.26	3.752	5.13	1.375
1.2+1.8	20.39	2.425	8.41	1.807	19.86	3.147	6.31	1.509
1.2	20.98	2.316	9.06	1.854	20.29	2.665	7.61	1.621

In addition, the bubble expansion corresponding to the triple-frequency combination with lower frequency and smaller frequency difference is significantly larger than that corresponding to the triple-frequency combination with higher frequency and larger frequency difference, and the maximal bubble radius in muscle generated by the 0.5+0.51+0.52 MHz combination is 1.10 times greater than that produced by the 1.2+1.8+2.4 MHz combination, and 1.09 times higher than that in urine. The maximum value of the bubble radius produced by the 1.2+1.8+2.4 MHz combination is 1.06 times that under the 1.8+2.4 MHz combination in the urine, and the bubble expansion under the triple-frequency combination is significantly larger than that under the dual-frequency combination when the highest frequency of the dual-frequency combination is the same as that of the triple-frequency combination, which is 1.06 times that in the muscle. When the dual-frequency combination's lowest frequency and the triple-frequency combination's lowest frequency are identical, the bubble expansion under the dual-frequency combination is significantly larger than that under the triple-frequency combination, and the maximum value of the bubble radius produced by the 1.2+1.8 MHz combination in the urine is 1.11 times as much as that under the 1.2+1.8+2.4 MHz combination, and 1.06 times as much as that in the muscle. When the single-frequency ultrasound frequency was the same as the highest frequency of the dual-frequency combination, the bubble expansion under the dual combination was

significantly greater than that under the single-frequency irradiation, and the maximum value of the bubble radius produced by the 1.8+2.4 MHz combination in the urine was 1.02 times higher than that under the 2.4 MHz irradiation, which was 1.05 times higher than that in muscle, and when the ultrasound's single-frequency matched the dual combination's lowest frequency, the double combination of bubble expansion was significantly smaller than that under single-frequency irradiation, with 1.2 MHz irradiation producing a maximum bubble radius in urine that was 1.04 times greater than that under the 1.2+1.8 MHz combination, and 1.02 times greater in muscle. For single-frequency ultrasound irradiation, the bubble expansion corresponding to the higher frequency was significantly smaller than that corresponding to the lower frequency, with the maximum bubble radius in urine produced by 1.2 MHz irradiation being 1.25 times that of 2.4 MHz irradiation, and only 1.17 times that of muscle.

Under the same irradiation combination of single-frequency or multi-frequency (dual and triple frequency), the corresponding R_{max}/R_{min} values corresponded to the following medium in descending order: urine, water, kidney, and muscle. For the triple-frequency combination, the corresponding R_{max}/R_{min} values of the four mediums gradually increased from small to large as the combination frequency varied from high to low, and the frequency difference varied from large into small. Among them, the maximum values of R_{max}/R_{min} in urine and muscle were 17.88 and 9.41 for the 0.5+0.51+0.52 MHz combination, respectively, and the minimum values of R_{max}/R_{min} were 8.80 and 4.75 for the 1.2+1.8+2.4 MHz combination in urine and muscle, respectively. A total of 2.4 MHz combination had a 2.03-fold increase in R_{max}/R_{min} values in urine and about 1.98-fold in muscle. Regarding the combinations of single, dual, and triple frequencies, the corresponding R_{max}/R_{min} values in the four mediums in ascending order corresponding to the irradiation frequencies of 2.4 MHz, 1.8+2.4 MHz, 1.2+1.8+2.4 MHz, 1.2+1.8 MHz, and 1.2 MHz; among them, the R_{max}/R_{min} values of the 2.4 MHz combination were 5.93 and 5.93 and 1.98 times higher in the urine and the muscle, respectively. The maximum values of the 2.4 MHz combination in urine and muscle were 5.93 and 3.72, respectively, and the minimum values of R_{max}/R_{min} for the 1.2 MHz combination in urine and muscle were 14.16 and 7.61, respectively; the 1.2 MHz combination showed a 2.39-fold increase in the R_{max}/R_{min} value in urine relative to that of the 2.4 MHz combination, and the value in muscle was about 2.05-fold.

Discussion

This work presents a numerical investigation and comparison of the maximum and minimum values of bubble radius and bubble collapse time utilizing multi-frequency excitation in liquids and tissues with the values obtained from single-frequency excitation. The final equilibrium bubble radius grows rapidly due to the rapid expansion of bubbles created by rectified mass double diffusion under multi-frequency excitation [37]. Since it is doubtful that the transient cavity will exist for more than one or two excitation cycles, this omission is not important. Additionally, under the adiabatic process assumption, heat transmission is disregarded. It is easy to account for this effect by changing the multidirectional exponent's value at maximal bubble expansion from 1.4 to 1.0, or an isothermal process. The maximal radius of the bubble is demonstrated to be overestimated by the isothermal assumption and underestimated by the adiabatic assumption [38]. Variations in temperature also have a significant impact on cavitation. The cavitation threshold in liquids decreases with increasing ambient temperature, although it increases somewhat in tissues [39]. Because the bubbles do not have enough time to undergo a thermal reaction before transient cavitation occurs, this effect was not consid-

ered in this work. In pulsed ultrasound applications like ultrasonic thrombolysis, the temperature rise is negligible even though multi-frequency excitation can raise it during tissue ablation due to greater transient cavitation [40]. Furthermore, because multi-frequency excitation reduces waveform distortion, it produces less sound absorption at the same strength as single-frequency modes [41].

Under single-frequency and combined multi-frequency irradiation, the oscillations of the bubbles exhibit both maximum expansion and minimum compression, suggesting that higher temperatures are generated inside the bubbles. Longer bubble collapse times, a lowering minimum bubble radius, and an increasing maximum bubble radius all contribute to an increase in the warmth and intensity of the bubble collapse (as indicated by R_{max}/R_{min} and t_c), which is especially advantageous for cavitation effects brought on by ultrasonic irradiation [42, 43]. Furthermore, there are variations in the impact of irradiation frequencies and different media on the bubble collapse time. The longer the R_{max}/R_{min} ratio for the same medium, regardless of single-frequency or multi-frequency combined irradiation, and vice versa, the shorter the bubble collapse time. For the four types of medium, the longest bubble collapse times under the same single-frequency or multi-frequency combination of irradiation are urine, water, kidney, and muscle. The intensity of bubble growth and collapse reduced as the medium surrounding the bubbles became more viscous.

The dynamics of bubbles are also strongly influenced by their interactions with one another. Neighboring bubbles are attracted or repelled by the radiation pressure produced by bubble oscillations when several bubbles of various radii are present. The acoustic wave's velocity and amplitude alter when bubbles spread through a liquid, and its attenuation and scattering are significantly increased [44-46]. Additionally, during multi-frequency excitation, intricate patterns can be observed in the sign and magnitude of the Bjerknes force between two bubbles [47,48].

Since bubble dynamics are nonlinear, the emergence of shock fronts or waveform distortions could be quite important. Because the bubble's response frequency is much lower than its resonance frequency, higher-order harmonics introduced to the distorted waveform have been shown with minimal impact on the occurrence of transient cavitation. The fundamental harmonic is thought to be the primary cause of transient cavitation [14,49,50]. Nevertheless, recent research indicates that taking nonlinear waveform distortions into account lowers the maximum bubble size at which transient cavitation occurs [51,52], suggesting that our simulations using perfect sinusoids may have overstated the maximum bubble radius. However, because of the decreased waveform distortion, the difference is negligible for multi-frequency excitation. This is particularly true at low frequencies and sound pressure, the bubble radius maximum anticipated by multi-frequency stimulation is more accurate than that predicted by single-frequency excitation.

Conclusion

In this paper, the nonlinear vibration of bubbles in the different mediums was simulated by using Gilmore-Akulichev and modified Keller-Miksis bubble dynamics equations and the dynamic change of bubble radius with time in the medium during multi-frequency combined ultrasonic irradiation was analyzed, and it was investigated how the frequency difference and multi-frequency ultrasonic combination affected the bubble collapse time as well as the bubble radius's maximum and minimum values. The effects of multi-frequency ultrasound combination and frequency difference on the maximum and minimum values of bubble radius and bubble extinction time in the different mediums were investigated, and this served as a guide for improving the multi-frequency ultrasonic combination to

lower the medium's transient threshold value. The simulation results demonstrate that the combination of the irradiation frequency and frequency difference is related to the bubble radius's maximum and lowest values in addition to the medium's characteristics. Where the highest ultrasound frequency is the same for single-frequency, dual-frequency, and triple-frequency combinations, the triple-frequency combination of irradiation under the bubble expansion is the largest and single-frequency irradiation under the bubble expansion is the smallest; when the lowest frequency combination of single-frequency, dual-frequency, and triple-frequency ultrasonography is the same, the triple-frequency combination of irradiation under the bubble expansion is the smallest, and single-frequency irradiation under the bubble expansion is the largest, and the bubble routing time is exactly proportional to the bubble collapse time, with the proportionality coefficient defined as the dimensionless radius ratio Rmax/Rmin (maximum to minimum bubble radius). This ratio characterizes the oscillation amplitude and correlates with nonlinear energy conversion efficiency [P8]. The triple-frequency combination with lower frequency and smaller frequency difference clearly has a larger bubble expansion radius maximum value than the triple-frequency combination with higher frequency and larger frequency difference maximum value. However, the minimum value of the bubble expansion radius is the exact opposite. The bubble collapse time has a positive relationship with the ratio of the maximum to minimum bubble expansion radius. In order to better control cavitation in the medium, the article's findings can help doctors choose the right frequency combination and frequency difference for multi-frequency ultrasound. They can also serve as a guide for designing tissue ablation treatment protocols and adjusting treatment parameters and irradiation dose during HIFU surgery.

Acknowledgment

The anonymous reviewers' insightful remarks and recommendations are much appreciated by the authors.

Authors' Contribution

H. Dong conceived and designed the research idea and framework; G. Liu performed the simulations; G. Peng analyzed the simulated data and wrote the manuscript. H. Dong revised the paper. All authors have read and agreed to the published version of the manuscript.

Ethical Approval

The School of Information Science and Engineering at Changsha Normal University has approved the research and use of necessary resources.

Funding

The Changsha Natural Science Foundation Project (grant No. kq2202313) and the Ministry of Education's Youth Fund Project of Humanities and Social Sciences Research (22YJCZH025) provided funding for this work.

Conflict of Interest

None

References

1. Song M, Sapozhnikov OA, Khokhlova VA, Khokhlova TD. Dynamic Mode Decomposition for Transient Cavitation Bubbles Imaging in Pulsed High-Intensity Focused Ultrasound Therapy. *IEEE Trans Ultrason Ferroelectr Freq Control.* 2024;**71**(5):596-606. doi: 10.1109/TUFFC.2024.3387351. PubMed PMID: 38598407. PubMed PMCID: PMC11141145.
2. Fu B, Shan D, Pu C, Guo L, Xu H, Peng C. A systematic investigation of thermal effects of high-intensity focused ultrasound therapy for ultrasound neuromodulation. *IEEE Transactions on Instrumentation and Measurement.* 2024;**73**:1-12. doi: 10.1109/TIM.2024.3366278.

3. McDannold N, Wen PY, Reardon DA, Fletcher SM, Golby AJ. Cavitation monitoring, treatment strategy, and acoustic simulations of focused ultrasound blood-brain barrier disruption in patients with glioblastoma. *J Control Release*. 2024;**372**:194-208. doi: 10.1016/j.jconrel.2024.06.036. PubMed PMID: 38897294. PubMed PMCID: PMC11299340.
4. Wang M, Zhang W, Chen Z, Paulus YM, Wang X, Yang X. Real-Time Cavitation Monitoring During Optical Coherence Tomography Guided Photo-Mediated Ultrasound Therapy of the Retina. *IEEE Trans Biomed Eng.* 2024;**71**(8):2473-2482. doi: 10.1109/TBME.2024.3377115. PubMed PMID: 38478443. PubMed PMCID: PMC11257808.
5. Iqbal MF, Shafique MA, Abdur Raqib M, Fadlalla Ahmad TK, Haseeb A, MA Mhjoob A, Raja A. Histotripsy: an innovative approach for minimally invasive tumour and disease treatment. *Ann Med Surg (Lond).* 2024;**86**(4):2081-7. doi: 10.1097/MS9.0000000000001897. PubMed PMID: 38576932. PubMed PMCID: PMC10990312.
6. Mustapha AT, Wahia H, Ji Q, Fakayode OA, Zhang L, Zhou C. Multiple-frequency ultrasound for the inactivation of microorganisms on food: A review. *Journal of Food Process Engineering*. 2024;**47**(4):e14587. doi: 10.1111/jfpe.14587.
7. Chen Z, Shen R, Xie J, Zeng Y, Wang K, Zhao L, et al. Multi-frequency ultrasonic-assisted enzymatic extraction of coconut paring oil from coconut by-products: Impact on the yield, physicochemical properties, and emulsion stability. *Ultrason Sonochem*. 2024;**109**:106996. doi: 10.1016/j.ultsonch.2024.106996. PubMed PMID: 39032371. PubMed PMCID: PMC11325078.
8. Diao X, Wang Y, Jia R, Chen X, Liu G, Liu D, Guan H. Influences of ultrasonic treatment on the physicochemical properties and microstructure of diacylglycerol-loaded emulsion stabilized with soybean protein isolate and sodium alginate. *Ultrason Sonochem.* 2024;**108**:106981. doi: 10.1016/j.ultsonch.2024.106981. PubMed PMID: 38981339. PubMed PMCID: PMC11280087.
9. Kumar S, Prajapat A, Panja SK, Shukla M. Ultrasound irradiation: fundamental theory, electromagnetic spectrum, important properties, and physical principles. In: Green Chemical Synthesis with Microwaves and Ultrasound. Weinheim: Wiley-VCH GmbH; 2024. p. 1-19.
10. Condezo-Hoyos L, Cortés-Avendaño P, Lama-Quispe S, Calizaya-Milla YE, Méndez-Albiñana P, Villamiel M. Structural, chemical and technofunctional properties pectin modification by green and novel intermediate frequency ultrasound procedure. *Ultrason Sonochem.* 2024;**102**:106743. doi: 10.1016/j.ultsonch.2023.106743. PubMed PMID: 38150956. PubMed PMCID: PMC10765486.
11. Moholkar VS, Rekveld S, Warmoeskerken MM. Modeling of the acoustic pressure fields and the distribution of the cavitation phenomena in a dual frequency sonic processor. *Ultrasonics*. 2000;**38**(1-8):666-70. doi: 10.1016/s0041-624x(99)00204-8. PubMed PMID: 10829749.
12. Tatake PA, Pandit AB. Modelling and experimental investigation into cavity dynamics and cavitational yield: influence of dual frequency ultrasound sources. *Chemical Engineering Science.* 2002;**57**(22-23):4987-95. doi: 10.1016/s0009-2509(02)00271-3.
13. Servant G, Laborde JL, Hita A, Caltagirone JP, Gérard A. On the interaction between ultrasound waves and bubble clouds in mono- and dual-frequency sonoreactors. *Ultrason Sonochem.* 2003;**10**(6):347-55. doi: 10.1016/S1350-4177(03)00105-6. PubMed PMID: 12927611.
14. Ye L, Zhu X, He Y, Song T. Effect of frequency ratio and phase difference on the dynamic behavior of a cavitation bubble induced by dual-frequency ultrasound. Chemical Engineering and Processing-Process *Intensification.* 2021;**165**:108448. doi: 10.1016/j.cep. 2021. 108448.
15. Brotchie A, Grieser F, Ashokkumar M. Sonochemistry and sonoluminescence under dual-frequency ultrasound irradiation in the presence of water-soluble solutes. *The Journal of Physical Chemistry C.* 2008;**112**(27):10247-50. doi: 10.1021/jp801763v.
16. Saletes I, Gilles B, Bera JC. Promoting inertial cavitation by nonlinear frequency mixing in a bifrequency focused ultrasound beam. *Ultrasonics*. 2011;**51**(1):94-101. doi: 10.1016/j.ultras.2010.06.003. PubMed PMID: 20637485.

17. Koufaki M, Fotopoulou T, Heropoulos GA. Synergistic effect of dual-frequency ultrasound irradiation in the one-pot synthesis of 3,5-disubstituted isoxazoles. *Ultrason Sonochem.* 2014;**21**(1):35-9. doi: 10.1016/j.ultsonch.2013.05.012. PubMed PMID: 23769747.
18. Suo D, Govind B, Zhang S, Jing Y. Numerical investigation of the inertial cavitation threshold under multi-frequency ultrasound. *Ultrason Sonochem*. 2018;**41**:419-26. doi: 10.1016/j.ultsonch.2017.10.004. PubMed PMID: 29137770.
19. Zhao X, Wang Z, Bai X, Cheng H, Ji B. Unsteady cavitation dynamics and pressure statistical analysis of a hydrofoil using the compressible cavitation model. *Physics of Fluids.* 2023;**35**(10):103307. doi: 10.1063/5.0164191.
20. Khanna S, Chakma S, Moholkar VS. Phase diagrams for dual frequency sonic processors using organic liquid medium. *Chemical Engineering Science.* 2013;**100**:137-44. doi: 10.1016/j.ces.2013.02.016.
21. Zhang Y, Billson D, Li S. Influences of pressure amplitudes and frequencies of dual-frequency acoustic excitation on the mass transfer across interfaces of gas bubbles. *International Communications in Heat and Mass Transfer.* 2015;**66**:167-71. doi: 10.1016/j.icheatmasstransfer.2015.05.026.
22. Guédra M, Inserra C, Gilles B. Accompanying the frequency shift of the nonlinear resonance of a gas bubble using a dual-frequency excitation. *Ultrason Sonochem*. 2017;**38**:298-305. doi: 10.1016/j.ultsonch.2017.03.028. PubMed PMID: 28633830.
23. Ye L, Zhu X, Liu Y. Numerical study on dual-frequency ultrasonic enhancing cavitation effect based on bubble dynamic evolution. *Ultrason Sonochem.* 2019;**59**:104744. doi: 10.1016/j.ultsonch.2019.104744. PubMed PMID: 31473426.
24. Azam SR, Ma H, Xu B, Devi S, Stanley SL, Siddique MA, et al. Multi-frequency multi-mode ultrasound treatment for removing pesticides from lettuce (Lactuca sativa L.) and effects on product quality. *Lwt.* 2021;**143**:111147. doi: 10.1016/j.lwt. 2021.111147.
25. Liao J, Tan J, Peng L, Xue H. Numerical investigation on the influence of dual-frequency coupling parameters on acoustic cavitation and its analysis of the enhancement and attenuation effect. *Ultrason Sonochem*. 2023;**100**:106614. doi: 10.1016/j.ultsonch.2023.106614. PubMed PMID: 37801994. PubMed PMCID: PMC10568426.
26. Wang X, Yan X, Min Q. Mass transfer of microbubble in liquid under multifrequency acoustic excitation - A theoretical study. *Ultrason Sonochem*. 2024;**102**:106760. doi: 10.1016/j.ultsonch.2024.106760. PubMed PMID: 38199078. PubMed PMCID: PMC10788794.
27. Wang M, Zhou Y. Numerical investigation of the inertial cavitation threshold by dual-frequency excitation in the fluid and tissue. *Ultrason Sonochem*. 2018;**42**:327-38. doi: 10.1016/j.ultsonch.2017.11.045. PubMed PMID: 29429677.
28. Carvell KJ, Bigelow TA. Dependence of cavitation bubble size on pressure amplitude at therapeutic levels. *AIP Conf Proc.* 2009;**1113**(1):63-67. doi: 10.1063/1.3131472.
29. Sojahrood AJ, Haghi H, Li Q, Porter TM, Karshafian R, Kolios MC. Nonlinear power loss in the oscillations of coated and uncoated bubbles: Role of thermal, radiation and encapsulating shell damping at various excitation pressures. *Ultrason Sonochem*. 2020;**66**:105070. doi: 10.1016/j.ultsonch.2020.105070. PubMed PMID: 32279052.
30. Filonets T, Solovchuk M, Sheu Tw. The Inertial Cavitation Threshold in Soft Tissue Using a Dual-Frequency Driving Signal. In: 14th WCCM-ECCOMAS Congress; 2021. p. 1-10
31. Abu-Nab AK, Mohamed KG, Abu-Bakr AF. An analytical approach for microbubble dynamics in histotripsy based on a neo-Hookean model. *Arch Appl Mech.* 2023;**93**(4):1565-77. doi: 10.1007/s00419-022-02346-4.
32. Gaudron R, Warnez MT, Johnsen E. Bubble dynamics in a viscoelastic medium with nonlinear elasticity. *Journal of Fluid Mechanics*. 2015;**766**:54-75. doi: 10.1017/jfm.2015.7.
33. Chu YM, Rehman MI, Khan MI, Nadeem S, Kadry S, Abdelmalek Z, Abbas N. Transportation of heat and mass transport in hydromagnetic stagnation point flow of Carreau nanomaterial: Dual simulations through Runge-Kutta Fehlberg technique. *International Communications in Heat and Mass Transfer.*

2020;**118**:104858. doi: 10.1016/j.icheatmasstransfer.2020.104858.

34. Noar NA, Apandi NI, Rosli N. A comparative study of Taylor method, fourth order Runge-Kutta method and Runge-Kutta Fehlberg method to solve ordinary differential equations. *AIP Conf Proc*. 2024;**2895**(1):020003. doi:10.1063/5.0192085.
35. Hong S, Son G. Numerical modelling of acoustic cavitation threshold in water with non-condensable bubble nuclei. *Ultrason Sonochem.* 2022;**83**:105932. doi: 10.1016/j.ultsonch.2022.105932. PubMed PMID: 35121570. PubMed PMCID: PMC8818585.
36. Church CC, Labuda C, Nightingale K. A theoretical study of inertial cavitation from acoustic radiation force impulse imaging and implications for the mechanical index. *Ultrasound Med Biol.* 2015;**41**(2):472-85. doi: 10.1016/j.ultrasmedbio.2014.09.012. PubMed PMID: 25592457. PubMed PMCID: PMC4297318.
37. Kolebaje OT, Vincent UE, Benyeogor BE, McClintock PVE. Effect of a modulated acoustic field on the dynamics of a vibrating charged bubble. *Ultrasonics*. 2023;**135**:107110. doi: 10.1016/j.ultras.2023.107110. PubMed PMID: 37499283.
38. Arienti M, Hwang J, Pickett L, Shekhawat Y. A thermally-limited bubble growth model for the relaxation time of superheated fuels. *International Journal of Heat and Mass Transfer.* 2020;**159**:120089. doi: 10.1016/j.ijheatmasstransfer.2020.120089.
39. Webb IR, Payne SJ, Coussios CC. The effect of temperature and viscoelasticity on cavitation dynamics during ultrasonic ablation. *J Acoust Soc Am.* 2011;**130**(5):3458-66. doi: 10.1121/1.3626136. PubMed PMID: 22088020.
40. Zhang D, Wang X, Lin J, Xiong Y, Lu H, Huang J, Lou X. Multi-frequency therapeutic ultrasound: A review. *Ultrason Sonochem*. 2023;**100**:106608. doi: 10.1016/j.ultsonch.2023.106608. PubMed PMID: 37774469. PubMed PMCID: PMC10543167.
41. Guo J, Zhang X, Fang Y, Qu R. An extremely-thin acoustic metasurface for low-frequency sound attenuation with a tunable absorption bandwidth. *International Journal of Mechanical Sciences*. 2022;**213**:106872. doi: 10.1016/j.ijmecsci.2021.106872.
42. Kanthale PM, Gogate PR, Pandit AB. Modeling aspects of dual frequency sonochemical reactors. *Chemical Engineering Journal.* 2007;**127**(1-3):71-9. doi: 10.1016/j.cej.2006.09.023.
43. Qin D, Lei S, Chen B, Li Z, Wang W, Ji X. Numerical investigation on acoustic cavitation characteristics of an air-vapor bubble: Effect of equation of state for interior gases. *Ultrason Sonochem.* 2023;**97**:106456. doi: 10.1016/j.ultsonch.2023.106456. PubMed PMID: 37271030. PubMed PMCID: PMC10251073.
44. Wang Z, Zhou W, Shu T, Xue Q, Zhang R, Wiercigroch M. Modelling of low-frequency acoustic wave propagation in dilute gas-bubbly liquids. *International Journal of Mechanical Sciences*. 2022;**216**:106979. doi: 10.1016/j.ijmecsci.2021.106979.
45. Ye Y, Song M, Liang Y, Li S, Dong C, Bu Z, Hu G. Numerical modelling and theoretical analysis of the acoustic attenuation in bubbly liquids. *Engineering Applications of Computational Fluid Mechanics.* 2023;**17**(1):2210193. doi: 10.1080/19942060.2023.2210193.
46. Gubaidullin DA, Fedorov YV. Acoustics of a viscoelastic medium with encapsulated bubbles. *J Hydrodyn.* 2021;**33**:55-62. doi: 10.1007/s42241-021-0003-2.
47. Wang X, Ning Z, Lv M, Yao J, Sun C. The secondary bjerknes force between two bubbles in ultrasonic field. *Journal of the Physical Society of Japan.* 2022;**91**(1):014401. doi: 10.7566/JPSJ.91.014401.
48. Zhang X, Li F, Wang C, Mo R, Hu J, Guo J, Lin S. Effects of translational motion on the Bjerknes forces of bubbles activated by strong acoustic waves. *Ultrasonics*. 2022;**126**:106809. doi: 10.1016/j.ultras.2022.106809. PubMed PMID: 35905527.
49. Beckwith C, Djambazov G, Pericleous K, Tonry C. Comparison of frequency domain and time domain methods for the numerical simulation of contactless ultrasonic cavitation. *Ultrason Sonochem.* 2022;**89**:106138. doi: 10.1016/j.ultsonch.2022.106138. PubMed PMID: 36049449. PubMed PMCID: PMC9441332.
50. Kashyap SR, Jaiman RK. Unsteady cavitation dynamics and frequency lock-in of a freely vibrating hydrofoil at high Reynolds num-

ber. *International Journal of Multiphase Flow.* 2023;**158**:104276. doi: 10.1016/j.ijmultiphaseflow.2022.10427.

51. Khavari M, Priyadarshi A, Morton J, Porfyrakis K, Pericleous K, Eskin D, Tzanakis I. Cavitation-induced shock wave behaviour in different liquids. *Ultrason Sonochem.* 2023;**94**:106328. doi: 10.1016/j.ultsonch.2023.106328. PubMed PMID: 36801674. PubMed PMCID: PMC9975297.

52. Kalmár P, Hegedűs F, Klapcsik K. A comparative study of measurements and numerical simulations of acoustically excited non-spherical bubbles oscillation. *International Journal of Multiphase Flow.* 2024;**179**:104947. doi: 10.1016/j.ijmultiphaseflow.2024.104947.